Interaction between residues in the Mg^{2+}-binding site regulates BK channel activation

Junqiu Yang,[1,2,3] Huanghe Yang,[2,3,4] Xiaohui Sun,[2,3,4] Kelli Delaloye,[2,3,4] Xiao Yang,[2,3,4] Alyssa Moller,[2,3,4] Jingyi Shi,[2,3,4] and Jianmin Cui[2,3,4]

[1]Department of Energy, Environmental and Chemical Engineering, [2]Cardiac Bioelectricity and Arrhythmia Center, [3]Center for the Investigation of Membrane Excitability Disorders, and [4]Department of Biomedical Engineering, Washington University, Saint Louis, MO 63130

As a unique member of the voltage-gated potassium channel family, a large conductance, voltage- and Ca^{2+}-activated K^+ (BK) channel has a large cytosolic domain that serves as the Ca^{2+} sensor, in addition to a membrane-spanning domain that contains the voltage-sensing (VSD) and pore-gate domains. The conformational changes of the cytosolic domain induced by Ca^{2+} binding and the conformational changes of the VSD induced by membrane voltage changes trigger the opening of the pore-gate domain. Although some structural information of these individual functional domains is available, how the interactions among these domains, especially the noncovalent interactions, control the dynamic gating process of BK channels is still not clear. Previous studies discovered that intracellular Mg^{2+} binds to an interdomain binding site consisting of D99 and N172 from the membrane-spanning domain and E374 and E399 from the cytosolic domain. The bound Mg^{2+} at this narrow interdomain interface activates the BK channel through an electrostatic interaction with a positively charged residue in the VSD. In this study, we investigated the potential interdomain interactions between the Mg^{2+}-coordination residues and their effects on channel gating. By introducing different charges to these residues, we discovered a native interdomain interaction between D99 and E374 that can affect BK channel activation. To understand the underlying mechanism of the interdomain interactions between the Mg^{2+}-coordination residues, we introduced artificial electrostatic interactions between residues 172 and 399 from two different domains. We found that the interdomain interactions between these two positions not only alter the local conformations near the Mg^{2+}-binding site but also change distant conformations including the pore-gate domain, thereby affecting the voltage- and Ca^{2+}-dependent activation of the BK channel. These results illustrate the importance of interdomain interactions to the allosteric gating mechanisms of BK channels.

INTRODUCTION

The large conductance, voltage- and Ca^{2+}-activated K^+ (BK) channel plays important roles in many physiological processes, such as muscle contraction, neural transmission, and circadian pacemaker output (Brayden and Nelson, 1992; Robitaille et al., 1993; Meredith et al., 2006). A functional BK channel is composed of four Slo1 subunits, each of which comprises multiple structural modules (Fig. 1, A and B): a membrane-spanning domain including the pore-gate (S5 and S6) and voltage-sensing domain (VSD; S1 to S4), and a large cytosolic domain that contains two Ca^{2+}-binding sites to serve as the Ca^{2+} sensor (Adelman et al., 1992; Schreiber and Salkoff, 1997; Xia et al., 2002; Zhang et al., 2010). Conformational changes of the VSD upon membrane depolarization and conformational changes of the cytosolic domain upon Ca^{2+} binding control BK channel activation.

Intracellular Mg^{2+} activates BK channels (Golowasch et al., 1986; Oberhauser et al., 1988; Shi and Cui, 2001; Zhang et al., 2001) by binding to the interface between the cytosolic and membrane-spanning domains (Shi et al., 2002; Xia et al., 2002; Yang et al., 2008). The Mg^{2+}-binding site is composed of residues E374 and E399 that are located in the cytosolic domain and D99 and N172 in the membrane-spanning domain (Fig. 1, A and B). The bound Mg^{2+} activates the channel by repulsing gating charge R213 in the voltage sensor S4 through an electrostatic interaction (Hu et al., 2003; Yang et al., 2007, 2008) (Fig. 1 A). On the other hand, the oxygen atoms from the four Mg^{2+}-coordination residues contribute to the formation of an octahedral sphere for Mg^{2+} binding with Mg-O internuclear distance ranging from 2 to 2.2 Å (Dudev and Lim, 2003). Nevertheless, it is not known whether these physically proximate coordination residues, three of which are

Correspondence to Jianmin Cui: jcui@wustl.edu

H. Yang's present address is Dept. of Physiology and Dept. of Biochemistry and Biophysics, Howard Hughes Medical Institute, University of California, San Francisco, San Francisco, CA 94143.

Abbreviations used in this paper: BK, large conductance, voltage- and Ca^{2+}-activated K^+; VSD, voltage-sensing domain.

The Rockefeller University Press $30.00
J. Gen. Physiol. Vol. 141 No. 2 217–228
www.jgp.org/cgi/doi/10.1085/jgp.201210794

acidic with negative charges, interact with one another in the absence of Mg^{2+}, and if such interactions indeed exist, how they contribute to the allosteric mechanism of BK channel gating in general.

In this study, we discovered that a native interdomain interaction between Mg^{2+}-coordination residues D99 and E374, located in the membrane-spanning domain and the cytosolic domains, respectively, inhibits the activation of the WT BK channel. Further analysis indicates that both D99 and E374 also interact with other residues to affect BK channel activation, making the function of this native interaction difficult to resolve. Therefore, to further study the effects of the interactions between Mg^{2+}-coordination residues on the structure and activation of BK channels, we engineered different charges at the position of neutral residue N172 in the Mg^{2+}-binding site. We found that the charges at position 172 sense the charges at residue 399, and this electrostatic interaction regulates fundamental aspects of BK channel activation, including voltage- and Ca^{2+}-dependent activation and the intrinsic open probability of the activation gate. Our current work thus suggests that interaction between Mg^{2+}-binding coordination residues participates in BK channel activation.

MATERIALS AND METHODS

Mutagenesis and expression

The mutations were made from the *mbr5* splice variant of *mSlo1* (provided by L. Salkoff, Washington University, St. Louis, MO) (Butler et al., 1993) (available from GenBank accession no. GI:347143) using overlap-extension PCR. The PCR-amplified regions for all the mutations were verified by sequencing. RNA was transcribed in vitro with T3 polymerase (Ambion) and injected into *Xenopus laevis* oocytes (stage IV–V), each with an amount of 0.05–50 ng. Experiments were performed after 2–5 d of incubation at 18°C. The procedures for harvesting oocytes and housing *Xenopus* were approved by the Washington University Animal Studies Committee and performed according to the protocols.

Electrophysiology

Inside-out patches were formed from oocyte membrane by borosilicate pipettes of 0.8–1.5-MΩ resistance. Macroscopic currents were recorded using a patch-clamp amplifier (Axopatch 200-B; Molecular Devices) and PULSE acquisition software (HEKA). The current signals were low-pass filtered at 10 kHz by the amplifier's four-pole Bessel filter and digitized with 20-µs intervals. The pipette (extracellular) solution comprised (mM): 140 potassium methanesulphonic acid, 20 HEPES, 2 KCl, and 2 $MgCl_2$, pH 7.2. Intracellular solutions contained: 140 mM potassium methanesulphonic acid, 20 mM HEPES, 2 mM KCl, 1 mM EGTA, and 22 mg/L 18C6TA, pH 7.2. $CaCl_2$ standard solution was added to obtain the desired free $[Ca^{2+}]$ from 1.0 to 112 µM, which was verified by a Ca^{2+}-sensitive electrode (Thermo Electron). The nominal 0-µM $[Ca^{2+}]_i$ solution contained an additional 4 mM EGTA with no added Ca^{2+}, and the free $[Ca^{2+}]$ is calculated to be ~0.5 nM. EGTA was excluded from the intracellular solution containing 200 µM $[Ca^{2+}]$. The treatment of MTS reagents or DTT was performed by perfusing the intracellular side of the excised patch for 5 min with the corresponding solution. Before each experiment, the nominal 0-µM $[Ca^{2+}]_i$ solution was used to dilute the stock MTS reagents (500×) or DTT (10×) to the final concentration of 1 mM (MTSES), 0.2 mM (MTSET), 1 mM (MTSACE), or 10 mM (DTT). The MTSET solution was freshly prepared right before each perfusion because its lifetime is ~10 min, whereas the MTSES and MTSACE solutions were prepared every 30 min. The DTT solution was freshly prepared and used for the day. G-V relations of the same mutation before and after chemical modifications were obtained using different groups of patches. All the experiments were performed at room temperature (22–24°C).

Analysis

The tail current amplitudes at −80 mV were measured to determine the relative conductance. Each G–V relation was normalized and fitted with the Boltzmann equation:

$$\frac{G}{G_{\max}} = \frac{1}{1+\exp\left(-\frac{ze(V-V_{1/2})}{kT}\right)}, \quad (1)$$

where $G/G_{\max}$ is the ratio of conductance to maximal conductance, z is the number of equivalent charges, e is the elementary charge, V is membrane potential, $V_{1/2}$ is the voltage where $G/G_{\max}$ reaches 0.5, k is Boltzmann's constant, and T is absolute temperature. Error bars in this paper represent SEM unless stated otherwise. Unpaired Student's t test or two-way ANOVA were performed to detect a significant difference among the results, and a p-value smaller than 5% is considered significant. A p-value of multiple comparison is adjusted using the Bonferroni correction. The sample size in statistical analysis is between 3 and 16 in this paper.

Open probability at negative voltages

The open probability at negative voltages was measured by single-channel recordings using patches containing hundreds of channels (Horrigan et al., 1999; Cui and Aldrich, 2000). The open probability measured at negative voltages is combined with the corresponding G-V relation to construct a P_o-V relation, which is fitted to the following model, based on the conceptual framework provided by Horrigan, Cui, and Aldrich (HCA; Horrigan et al., 1999):

$$P_o = \frac{1}{1+\frac{\exp\left(-\frac{z_L FV}{RT}\right)}{L_o}\left(\frac{1+\exp\left(\frac{z_J F(V-V_{hc})}{RT}\right)}{1+\exp\left(\frac{z_J F(V-V_{ho})}{RT}\right)}\right)^4}, \quad (2)$$

where z_L is the charge associated with gate opening when all the voltage sensors are at their resting state, z_J is the charge associated with voltage-sensor movements, and L_0 is the intrinsic open probability at $V = 0$ while all the voltage sensors are at their resting state. V_{hc} and V_{ho} are the voltages for half of the voltage sensors to be at their activation state at the closed and the open conformations of the gate, respectively (Horrigan and Aldrich, 2002).

RESULTS

A native interdomain interaction within the Mg^{2+}-binding site participates in channel activation

To probe the native interaction that might exist between negatively charged D99 and E374/E399, we introduced positively charged Arg mutation to each of these residues and tested their perturbation on channel

activity. We found that, in the absence of Ca^{2+} and Mg^{2+}, the charge-reversal mutation of either D99 or E374, but not E399, enhances channel activation, as indicated by the shifts of the G-V relation to lower voltage range (Fig. 1, C–E). To test whether the activating effects of single mutations of D99R and E374R are dependent on each other, we measured the activation of the double mutation D99R/E374R. The G-V relation of the combined mutation D99R/E374R returns to a similar position of the WT channel (Fig. 1, D and E), indicating that the effects of D99R and E374R are not independent and that this double mutation containing two positive charges abolishes the activating effects of the single mutation of D99R or E374R. Therefore, our mutagenesis studies suggest that D99 and E374 interact with each other to participate in channel activation.

To examine if the interaction between D99 and E374 depends on electric charges, we measured the effect of E374R on the G-V relation in the background of mutation D99A; E374R has a smaller effect on the G-V relation (Fig. 1 E), consistent with an electrostatic interaction between D99 and E374.

During further study of this interdomain interaction, we found that residues D99 and E374 are involved in interactions with other sites such as R213 in the voltage sensor S4 (unpublished data). To further understand the role of the interdomain interaction within the Mg^{2+}-binding site in channel activation without the interference of other types of interactions, we engineered artificial electrostatic interactions between residues at positions 172 and 399 and characterized the effects of these interactions in the remaining part of this work.

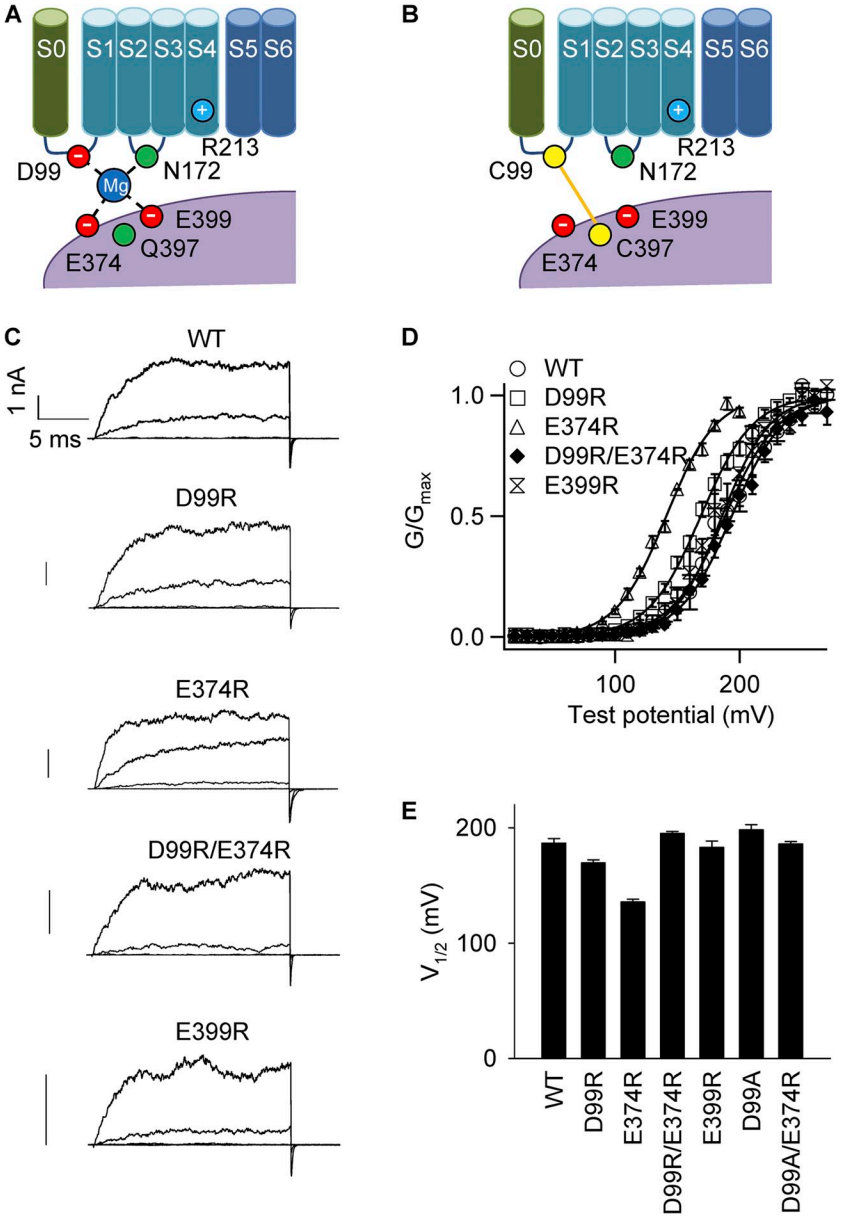

Figure 1. D99 and E374 interact with each other at the domain interface of BK channels. (A) Cartoon showing the molecular mechanism of Mg^{2+} activation. S0–S6 are membrane-spanning segments. Mg^{2+} is coordinated by four residues including D99 and N172 from the membrane-spanning domain and E374 and E399 from the cytosolic domain. Bound Mg^{2+} interacts with R213 of the membrane-spanning domain to activate channel. Located in the vicinity of the Mg^{2+}-binding site is residue Q397, which may interact with R213 when charged. (B) Cartoon showing the spontaneous formation of a disulfide bond between C99 and C397 located in the membrane-spanning and cytosolic domains, respectively. (C) Macroscopic current traces of inside-out patches expressing WT BK channels and D99R, E374R, D99R/E374R, and E399R mutant channels. Currents were elicited by voltages ranging from 0 to 200 mV, with 50-mV increments. The voltage was −50 mV before and −80 mV after the pulses. $[Ca^{2+}]_i$: 0 µM. Bars, 1 nA. (D) G-V relations of WT, D99R, E374R, D99R/E374R, and E399R. $[Ca^{2+}]_i$: 0 µM. Solid lines are fittings to the Boltzmann equation. The fitting parameters are: WT (n = 4): $V_{1/2}$ = 187 ± 4 and z = 1.29 ± 0.12; D99R (n = 14): $V_{1/2}$ = 170 ± 3 and z = 1.31 ± 0.03; E374R (n = 6): $V_{1/2}$ = 136 ± 2 and z = 1.29 ± 0.04; D99R/E374R (n = 5): $V_{1/2}$ = 195 ± 2 and z = 1.21 ± 0.05; E399R (n = 3): $V_{1/2}$ = 183 ± 5 and z = 1.34 ± 0.10. (E) $V_{1/2}$ of the G-V relations. The fitting parameters for D99A and D99A/E374R are: D99A (n = 6): $V_{1/2}$ = 198 ± 5 and z = 1.20 ± 0.05; D99A/E374R (n = 7): $V_{1/2}$ = 186 ± 2 and z = 1.24 ± 0.06.

Electrostatic interactions between residues 172 and 399 alter channel activation

As is the case with the residue pair of D99 and E374, N172 and E399 are also part of the Mg^{2+}-binding site (Shi et al., 2002; Yang et al., 2008) (Fig. 1, A and B). Shifts of the G-V curves to more positive voltages were observed when we introduced an artificial electrostatic interaction between positions 172 and 399 by modifying the double cysteine mutation (N172C/E399C) with charged MTS reagents, MTSET(+) and MTSES(−) (Fig. 2, A and B). Neither MTSET nor MTSES affects the control channel (C430A; Fig. 2 C), indicating that these MTS reagents react with the cysteines on residues 172 and 399. In contrast to the effect of MTSET(+) and MTSES(−), modification with neutral MTSACE did not affect the G-V relation of N172C/E399C (Fig. 2 D). Moreover, a subsequent MTSET(+) treatment failed to shift the G-V relation, indicating that both C172 and C399 were covalently modified by neutral MTSACE so that no free thiol groups at these two positions were available to react with MTSET(+). These results suggest that the engineered two charges with the same sign at 172 and 399 hinder channel activation through electrostatic repulsion with each other. Consistent with this mechanism, the effects of the charged MTS reagents on channel activation in 200 μM Ca^{2+} were attenuated in 1 M NaCl intracellular solution (Fig. 3, C and D), indicating that increasing ionic strength indeed weakens the electrostatic repulsion between these two sites. The osmolarity change brought by 1 M NaCl has no effect on BK channel activation, as shown previously (Yang et al., 2010). Although ionic strength also affects WT channel activation in other $[Ca^{2+}]_i$, the increase of ionic strength in 200 μM Ca^{2+} had no effect on control channel activation (Fig. 3, A and B). Therefore, the effect of the charged MTS reagents on channel activation is caused by electrostatic interactions that are sensitive to the change of ionic strength of the solution.

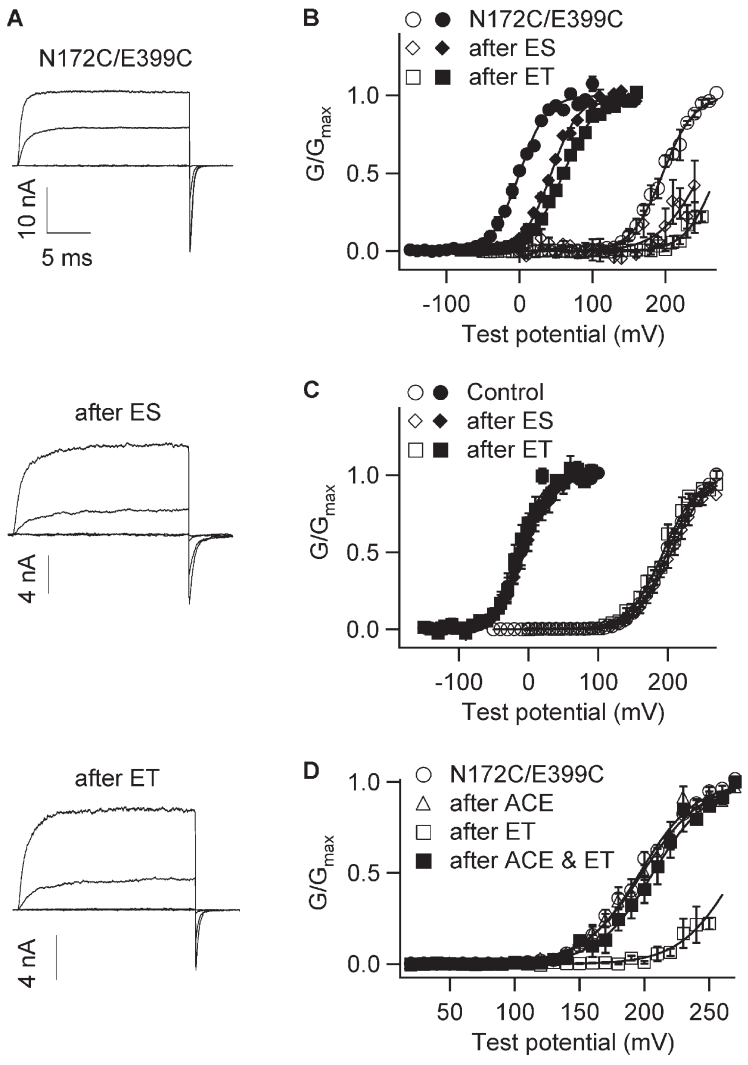

Figure 2. Electrostatic repulsion between residues 172 and 399 inhibits channel activation. (A) Macroscopic current traces of inside-out patches expressing N172C/E399C before and after treatment of negative MTSES(−) (ES) or positive MTSET(+) (ET) reagent. Currents were elicited by voltages of −50, 0, 50, and 100 mV. The voltage was −50 mV before and −120 mV (top) or −80 mV (middle and bottom) after the pulses. $[Ca^{2+}]_i$: 200 μM. (B) G-V relation of N172C/E399C shifts after treatment of ES or ET reagent. Open symbols, $[Ca^{2+}]_i$: 0 μM; closed symbols, $[Ca^{2+}]_i$: 200 μM. Solid lines are fittings to the Boltzmann equation. The fitting parameters are: N172C/E399C untreated, 0 $[Ca^{2+}]_i$ ($n = 3$): $V_{1/2} = 197 \pm 5$ and $z = 1.19 \pm 0.22$; 200 μM $[Ca^{2+}]_i$ ($n = 7$): $V_{1/2} = 2 \pm 7$ and $z = 1.20 \pm 0.09$; after MTSES treatment, 0 $[Ca^{2+}]_i$ ($n = 3$): $V_{1/2} = 250 \pm 25$ and $z = 0.86 \pm 0.60$; 200 μM $[Ca^{2+}]_i$ ($n = 7$): $V_{1/2} = 47 \pm 6$ and $z = 1.13 \pm 0.27$; after MESET treatment, 0 $[Ca^{2+}]_i$ ($n = 3$): $V_{1/2} = 271 \pm 10$ and $z = 1.19 \pm 0.44$; 200 μM $[Ca^{2+}]_i$ ($n = 4$): $V_{1/2} = 61 \pm 1$ and $z = 1.13 \pm 0.03$. (C) G-V relation of the control C430A after treatment of ES or ET reagent. Open symbols: $[Ca^{2+}]_i$: 0 μM; closed symbols: $[Ca^{2+}]_i$: 200 μM. Solid lines are fittings to the Boltzmann equation. The fitting parameters are: C430A untreated, 0 $[Ca^{2+}]_i$ ($n = 7$): $V_{1/2} = 198 \pm 2$ and $z = 1.13 \pm 0.03$; 200 μM $[Ca^{2+}]_i$ ($n = 6$): $V_{1/2} = -19 \pm 4$ and $z = 1.48 \pm 0.08$; after MTSES treatment, 0 $[Ca^{2+}]_i$ ($n = 6$): $V_{1/2} = 204 \pm 6$ and $z = 1.11 \pm 0.04$; 200 μM $[Ca^{2+}]_i$ ($n = 3$): $V_{1/2} = -7 \pm 4$ and $z = 1.26 \pm 0.15$; after MESET treatment, 0 $[Ca^{2+}]_i$ ($n = 3$): $V_{1/2} = 195 \pm 2$ and $z = 1.09 \pm 0.06$; 200 μM $[Ca^{2+}]_i$ ($n = 3$): $V_{1/2} = -14 \pm 6$ and $z = 1.54 \pm 0.49$. (D) G-V relations of N172C/E399C after treatment of neutral MTSACE (ACE) and/or positive ET. $[Ca^{2+}]_i$: 0 μM. Solid lines are fittings to the Boltzmann equation. The fitting parameters are: N172C/E399C untreated ($n = 3$): $V_{1/2} = 197 \pm 5$ and $z = 1.19 \pm 0.22$; after MTSACE treatment ($n = 4$): $V_{1/2} = 199 \pm 5$ and $z = 1.11 \pm 0.21$; after MTSET treatment ($n = 3$): $V_{1/2} = 271 \pm 10$ and $z = 1.19 \pm 0.44$; after MTSACE and MTSET treatments ($n = 3$): $V_{1/2} = 207 \pm 4$ and $z = 1.19 \pm 0.22$. N172C/E399C mutation is on the background of C430A to eliminate the effects of MTS reagents on the native C430 (Zhang and Horrigan, 2005).

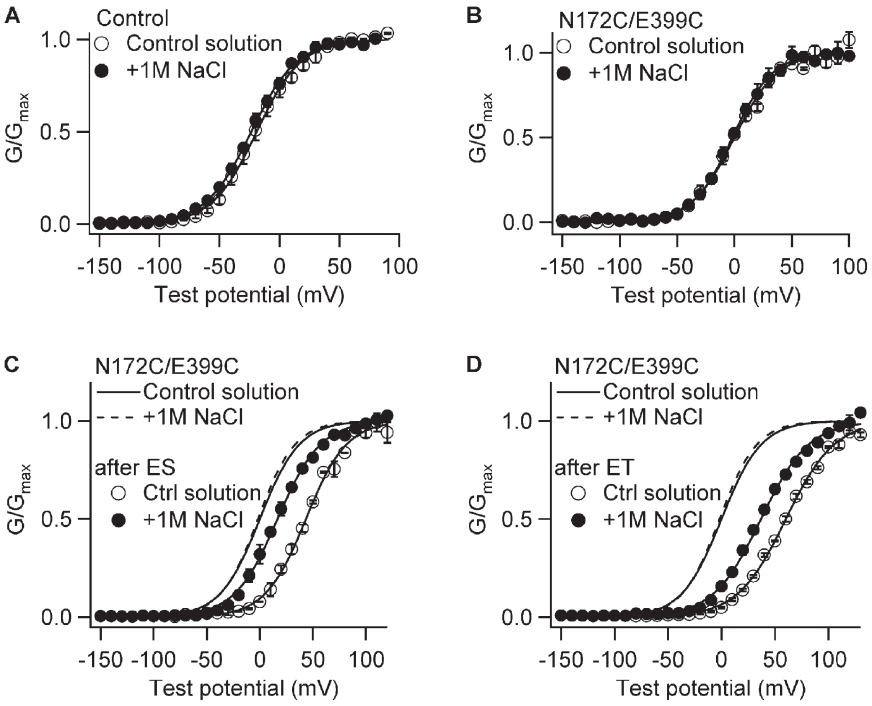

Figure 3. Electrostatic interactions between residues 172 and 399 depend on ionic strength. (A–D) G-V relations in control solution (200 μM $[Ca^{2+}]_i$ solution) or in control solution with an additional 1 M NaCl for the control (A), N172C/E399C (B), N172C/E399C after MTSES (C), or N172C/E399C after MTSET (D). All G-V curves are fitted to the Boltzmann equation (lines). The fitting parameters are: the control channel under control solution ($n = 6$): $V_{1/2} = -19 \pm 4$ and $z = 1.48 \pm 0.08$; under an additional 1 M NaCl ($n = 3$): $V_{1/2} = -24 \pm 3$ and $z = 1.36 \pm 0.08$; N172C/E399C under control solution ($n = 7$): $V_{1/2} = 2 \pm 7$ and $z = 1.20 \pm 0.09$; under an additional 1 M NaCl ($n = 8$): $V_{1/2} = 3 \pm 7$ and $z = 1.32 \pm 0.07$; N172C/E399C after MTSES under control solution ($n = 2$): $V_{1/2} = 43 \pm 1$ and $z = 1.32 \pm 0.11$; under an additional 1 M NaCl ($n = 3$): $V_{1/2} = 17 \pm 2$ and $z = 1.29 \pm 0.05$; N172C/E399C after MTSET under control solution ($n = 4$): $V_{1/2} = 60 \pm 1$ and $z = 1.13 \pm 0.03$; under an additional 1 M NaCl ($n = 4$): $V_{1/2} = 39 \pm 2$ and $z = 1.14 \pm 0.03$. The control and N172C/E399C mutation are on the background of C430A.

Compared with the native D99–E374 interaction, the advantage of studying the 172–399 interaction is that varying charge type at residue 399 had no obvious effect on channel activation when residue 172 remained neutral (Fig. 4 A). This suggests that the charges at residue 399 affect channel activation only when an electrostatic interaction is established with the charges at residue 172. On the other hand, the effects of charges at residue 172 are more complicated because varying charge type at residue 172 still was able to change the G-V relation when residue 399 was neutral (Fig. 4 B). This suggests that the charges at residue 172 probably interact with other charges besides E399. By testing the voltage at half-maximum of G-V relation ($V_{1/2}$) against the charge type at 172 and 399 for 26 mutations and chemical modifications, ANOVA detects a significant difference among the $V_{1/2}$ values with different charge type at residue 172 ($P = 0.049$) but not with the charge type at residue 399 ($P = 0.364$) (Fig. 4 C and Table 1). However, although charges at 399 do not interact with other charges, the

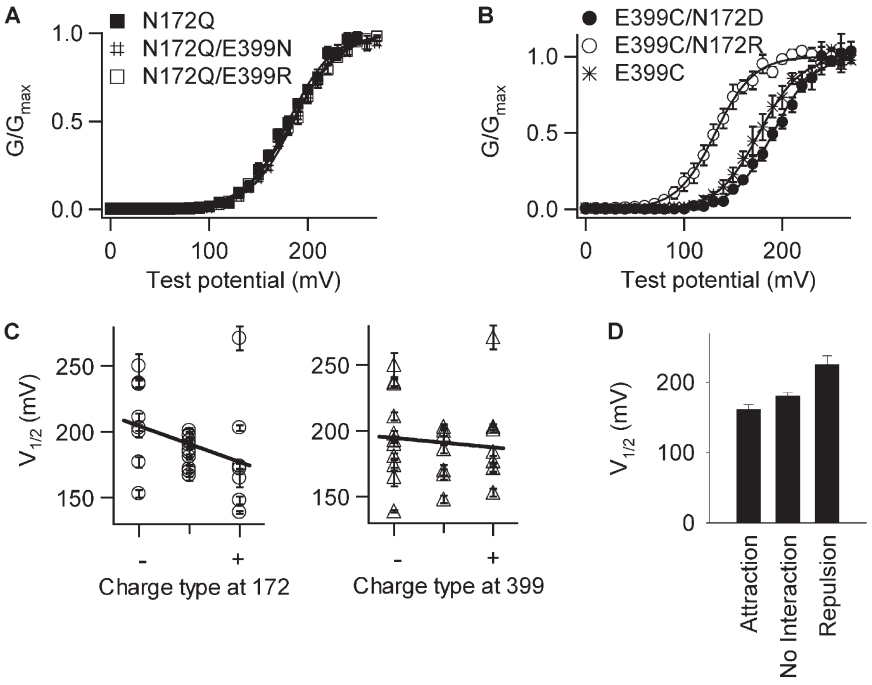

Figure 4. Effects of charge type at residues 172 and 399 on channel activation. G-V relation is shifted by charge type at residue 172 (B) but not by residue 399 (A). $[Ca^{2+}]_i$: 0. Solid lines are fittings to the Boltzmann equation. The fitting parameters are: N172Q ($n = 4$): $V_{1/2} = 181 \pm 5$ and $z = 1.11 \pm 0.20$; N172Q/E399N ($n = 5$): $V_{1/2} = 186 \pm 4$ and $z = 1.15 \pm 0.18$; N172Q/E399R ($n = 5$): $V_{1/2} = 184 \pm 4$ and $z = 1.04 \pm 0.17$; E399C/N172D ($n = 8$): $V_{1/2} = 188 \pm 4$ and $z = 1.23 \pm 0.23$; E399C/N172R ($n = 5$): $V_{1/2} = 132 \pm 5$ and $z = 1.30 \pm 0.29$; E399C ($n = 6$): $V_{1/2} = 201 \pm 4$ and $z = 1.23 \pm 0.22$. (C) $V_{1/2}$ of a variety of N172 and E399 mutations with or without chemical modifications listed in Table 1 versus charge type at 172 (left) or 399 (right). Solid lines are fittings to linear regression. The slope ± fitting SD of linear regression is -16.1 ± 7.5 for the charge type at 172 and -2.6 ± 7.4 for the charge type at 399. (D) $V_{1/2}$'s of mutations in Table 1 are averaged based on the interaction type between 172 and 399.

data in Table 1 suggest that charges at 399 affect channel activation by interacting with the charges at 172 because ANOVA shows that the interaction between 172 and 399 affects channel activation with a p-value of 0.0006 (Fig. 4 D and Table 1).

Thus, channel activation is altered by the electrostatic interaction between the charges at residues 172 and 399. Different types of interaction—repulsion, attraction, or no interaction—can be introduced to cause different effects on channel activation. To avoid the complication of varying the charge at 172, which interacts with other charges in addition to that at 399, we changed the interaction type by varying the charge at 399 and keeping the same residue at 172 for each set of the following experiments.

Electrostatic interaction between residues 172 and 399 alters voltage and Ca^{2+} dependence

BK channels are activated by voltage and Ca^{2+} via distinct allosteric mechanisms (Horrigan and Aldrich, 2002; Cui et al., 2009). Would interactions between the Mg^{2+}-coordination residues specifically alter voltage or Ca^{2+}-dependent activation, or do such interactions affect both mechanisms? To address this question, we examined the voltage-dependent activation (measured as $V_{1/2}$ of the G-V relation in 0 $[Ca^{2+}]_i$) and Ca^{2+}-dependent activation (measured as shift of the G-V, $\Delta V_{1/2}$, caused by an increase of $[Ca^{2+}]_i$ from 0 to the saturating 112 µM) for several mutations and found that both are affected by the 172–399 electrostatic interactions (Fig. 5). Mutations of E399 to neutral (C or N) and positive charge (R) altered both voltage (Fig. 5 A) and Ca^{2+} (Fig. 5 B) -dependent activation on the background of N172R or N172D, but had no effect on channel activation on the background of WT or N172Q where residue 172 is neutral. Interestingly, the results show that regardless of the charge type at residues 172 or 399, a repulsive 172–399 interaction shifted the voltage dependence to higher voltage ranges (Fig. 5 A) and increased Ca^{2+} sensitivity (Fig. 5 B) as compared with that of an attractive 172–399 interaction in

TABLE 1

$V_{1/2}$ of G-V relation for a variety of mutations with or without MTS modification

No.	Charge at 172	Charge at 399	Interaction	$V_{1/2}$
				mV
1	0 (Cys)	0 (Cys)	0	197 ± 5
2	− (Cys/ES)	− (Cys/ES)	Rep	250 ± 9
3	+ (Cys/ET)	+ (Cys/ET)	Rep	271 ± 9
4	0 (Cys)	− (Glu)	0	193 ± 2
5	− (Cys/ES)	− (Glu)	Rep	236 ± 3
6	+ (Cys/ET)	− (Glu)	Attr	174 ± 4
7	0 (Asn)	0 (Cys)	0	167 ± 4
8	0 (Asn)	− (Cys/ES)	0	190 ± 2
9	0 (Asn)	+ (Cys/ET)	0	201 ± 2
10	− (Asp)	0 (Cys)	0	203 ± 2
11	− (Asp)	− (Cys/ES)	Rep	237 ± 3
12	− (Asp)	+ (Cys/ET)	Attr	177 ± 4
13	+ (Arg)	0 (Cys)	0	148 ± 3
14	+ (Arg)	− (Cys/ES)	Attr	165 ± 7
15	+ (Arg)	+ (Cys/ET)	Rep	203 ± 2
16	0 (Asn)	− (Glu)	0	198 ± 2
17	+ (Arg)	− (Glu)	Attr	139 ± 1
18	+ (Arg)	+ (Arg)	Rep	172 ± 4
19	− (Asp)	− (Glu)	Rep	211 ± 3
20	− (Asp)	0 (Asn)	0	200 ± 4
21	− (Asp)	+ (Arg)	Attr	153 ± 3
22	0 (Asn)	0 (Asn)	0	170 ± 4
23	0 (Asn)	+ (Arg)	0	172 ± 3
24	0 (Gln)	− (Glu)	0	181 ± 2
25	0 (Gln)	0 (Asn)	0	186 ± 3
26	0 (Gln)	+ (Arg)	0	184 ± 3
P	0.049[a]	0.364	0.0006[a]	

The charge type is listed for each mutation using symbols (+, positive; −, negative; 0, neutral), along with the amino acid and MTS reagent. As a result, the electrostatic interaction between 172 and 399 can be repulsion (Rep, between like charges), attraction (Attr, between opposite charges), or 0 (not both are charged). The p-values are calculated using ANOVA test (see Materials and methods). Mutations 1–18 are on the background of C430A.

[a]A p-value of <0.05 indicates that a significant difference among the $V_{1/2}$ values was detected with different charge or interaction type.

the same group. This result is similar to that of the native interaction between D99 and E374 (Fig. 1).

The effect of 172–399 interactions on Ca^{2+}-dependent activation is not limited to the activation by saturating Ca^{2+} concentration; it also affects the activation by intermediate Ca^{2+} concentration. Fig. 5 (C–E) shows the G-V relations with varying $[Ca^{2+}]_i$ ranging from 0 to 112 μM for mutations of E399 to C or R on the background of N172R. The mutations change the 172–399 interaction from attraction to none or repulsion. With increasing $[Ca^{2+}]_i$, the G-V relations shift on the voltage axis with approximately equal intervals for N172R (Fig. 5, C and F) but with larger intervals at low $[Ca^{2+}]_i$ for N172R/E399R, such that the G-V curves cluster at high $[Ca^{2+}]_i$ (Fig. 5, E and F). Consistently, the distribution of G-V curves of N172R/E399C shows intermediate distribution along the voltage axis (Fig. 5, D and F). On the other hand, the slope of G-V relations does not vary significantly at different $[Ca^{2+}]_i$ or among different mutant channels (Fig. 5, C–F). These results indicate that the BK channel becomes more sensitive to both saturating and intermediate $[Ca^{2+}]_i$ when the 172–399 interaction changes from attraction to repulsion. Based on the above experiments, we conclude that both voltage- and

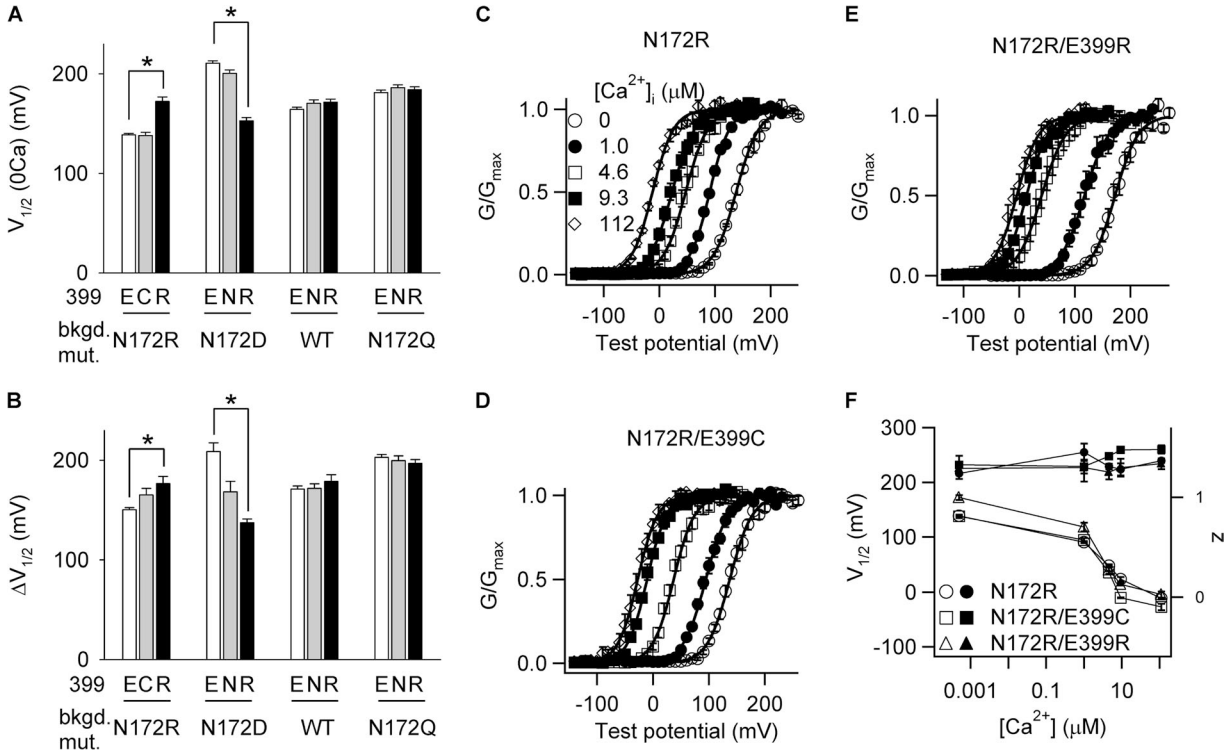

Figure 5. The 172–399 electrostatic interaction alters voltage- and Ca^{2+}-dependent activation. (A) $V_{1/2}$ at 0 $[Ca^{2+}]_i$ indicating changes in voltage-dependent activation. The mutations are grouped such that the negative residue E399 (open bars) is mutated to neutral (gray bars) or positive (closed bars) residues on the backgrounds where residue 172 contains a negative, positive, or no charge. (B) $\Delta V_{1/2}$ = $V_{1/2}$ at 0 $[Ca^{2+}]_i$ − $V_{1/2}$ at 112 μM $[Ca^{2+}]_i$, indicating Ca^{2+} activation by saturating $[Ca^{2+}]_i$. Mutations are the same as in A. Asterisks in A and B indicate significant difference between the labeled pairs as identified in multiple comparisons ($P < 0.017$ as adjusted by the Bonferroni correction). The group of N172R mutations in A and B are made on the background of C430A. There is no significant difference in the number of equivalent gating charges among all the G-V relations. (C–E) G-V relation for N172R (C), N172R/E399C (D), and N172R/E399R (E) in varying $[Ca^{2+}]_i$. Solid lines are fittings to the Boltzmann equation. The fitting parameters of the mutations in A–E are: N172R 0 Ca ($n = 4$): $V_{1/2} = 139 \pm 1$ and $z = 1.24 \pm 0.05$; 1.0 Ca ($n = 4$): $V_{1/2} = 91 \pm 2$ and $z = 1.45 \pm 0.09$; 4.6 Ca ($n = 4$): $V_{1/2} = 48 \pm 3$ and $z = 1.31 \pm 0.03$; 9.3 Ca ($n = 4$): $V_{1/2} = 23 \pm 4$ and $z = 1.28 \pm 0.06$; 112 Ca ($n = 3$): $V_{1/2} = -12 \pm 2$ and $z = 1.37 \pm 0.02$; N172R/E399C 0 Ca ($n = 6$): $V_{1/2} = 138 \pm 3$ and $z = 1.33 \pm 0.09$; 1.0 Ca ($n = 5$): $V_{1/2} = 95 \pm 3$ and $z = 1.31 \pm 0.07$; 4.6 Ca ($n = 4$): $V_{1/2} = 36 \pm 2$ and $z = 1.41 \pm 0.03$; 9.3 Ca ($n = 2$): $V_{1/2} = -10 \pm 1$ and $z = 1.48 \pm 0.02$; 112 Ca ($n = 3$): $V_{1/2} = -27 \pm 6$ and $z = 1.48 \pm 0.04$; N172R/E399R 0 Ca ($n = 4$): $V_{1/2} = 172 \pm 4$ and $z = 1.29 \pm 0.05$; 1.0 Ca ($n = 4$): $V_{1/2} = 118 \pm 8$ and $z = 1.30 \pm 0.14$; 4.6 Ca ($n = 4$): $V_{1/2} = 41 \pm 4$ and $z = 1.25 \pm 0.07$; 9.3 Ca ($n = 4$): $V_{1/2} = 14 \pm 2$ and $z = 1.30 \pm 0.09$; 112 Ca ($n = 3$): $V_{1/2} = -4 \pm 6$ and $z = 1.34 \pm 0.05$; N172D 0 Ca ($n = 4$): $V_{1/2} = 204 \pm 4$ and $z = 1.18 \pm 0.20$; 112 Ca ($n = 3$): $V_{1/2} = 20 \pm 5$ and $z = 0.96 \pm 0.15$; N172D/E399N 0 Ca ($n = 10$): $V_{1/2} = 200 \pm 4$ and $z = 1.26 \pm 0.07$; 112 Ca ($n = 2$): $V_{1/2} = 32 \pm 10$ and $z = 1.34 \pm 0.04$; N172D/E399R 0 Ca ($n = 4$): $V_{1/2} = 153 \pm 3$ and $z = 1.28 \pm 0.07$; 112 Ca ($n = 4$): $V_{1/2} = 16 \pm 2$ and $z = 1.02 \pm 0.02$; WT 0 Ca ($n = 7$): $V_{1/2} = 164 \pm 2$ and $z = 1.18 \pm 0.05$; 112 Ca ($n = 5$): $V_{1/2} = -7 \pm 2$ and $z = 1.55 \pm 0.07$; E399N 0 Ca ($n = 9$): $V_{1/2} = 170 \pm 4$ and $z = 1.18 \pm 0.03$; 112 Ca ($n = 5$): $V_{1/2} = -1 \pm 3$ and $z = 1.59 \pm 0.07$; E399R 0 Ca ($n = 7$): $V_{1/2} = 172 \pm 3$ and $z = 1.30 \pm 0.09$; 112 Ca ($n = 7$): $V_{1/2} = -7 \pm 6$ and $z = 1.52 \pm 0.05$; N172Q 0 Ca ($n = 4$): $V_{1/2} = 181 \pm 2$ and $z = 1.11 \pm 0.09$; 112 Ca ($n = 5$): $V_{1/2} = -22 \pm 2$ and $z = 1.42 \pm 0.05$; N172Q/E399N 0 Ca ($n = 5$): $V_{1/2} = 186 \pm 3$ and $z = 1.11 \pm 0.07$; 112 Ca ($n = 4$): $V_{1/2} = -14 \pm 4$ and $z = 1.43 \pm 0.05$; N172Q/E399R 0 Ca ($n = 5$): $V_{1/2} = 184 \pm 3$ and $z = 1.10 \pm 0.02$; 112 Ca ($n = 4$): $V_{1/2} = -13 \pm 3$ and $z = 1.46 \pm 0.07$. All these mutations are on the C430A background. (F) $V_{1/2}$ (open symbols) and z (closed symbols) versus $[Ca^{2+}]_i$ for the G-V relations in C–E.

Ca^{2+}-dependent activation are altered by the electrostatic interaction between residues 172 and 399.

Electrostatic interaction between residues 172 and 399 alters local conformation

Because the Mg^{2+}-binding site is not near the Ca^{2+}-binding site according to the recent crystal structures of the cytosolic domain (Y. Wu et al., 2010; Yuan et al., 2010, 2012), the interaction between residues 172 and 399 has to alter the Ca^{2+}-dependent activation through allosteric effects. To understand the underlying structural mechanism causing these allosteric effects, we first tested whether the 172–399 interaction could alter local conformation in the vicinity of the Mg^{2+}-binding site. The effect of 172–399 electrostatic interactions on the spontaneous formation of a disulfide bond between C99 and C397 (Yang et al., 2008) was monitored. Residues 99 and 397 are located in the vicinity of residues 172 and 399. Previously, we have shown that cysteines at these two residues spontaneously form a disulfide bond (Fig. 1 B) (Yang et al., 2008). The formation of disulfide bonds requires proper orientation of the two cysteine residues and the distance between the C_β atoms of the two cysteine residues to be within the range of 2.9 to 4.6 Å (Hazes and Dijkstra, 1988). If the 172–399 interaction alters the C_β–C_β distance to be outside of this range or changes their relative orientation, the formation of the disulfide bond would be prevented. Our previous studies

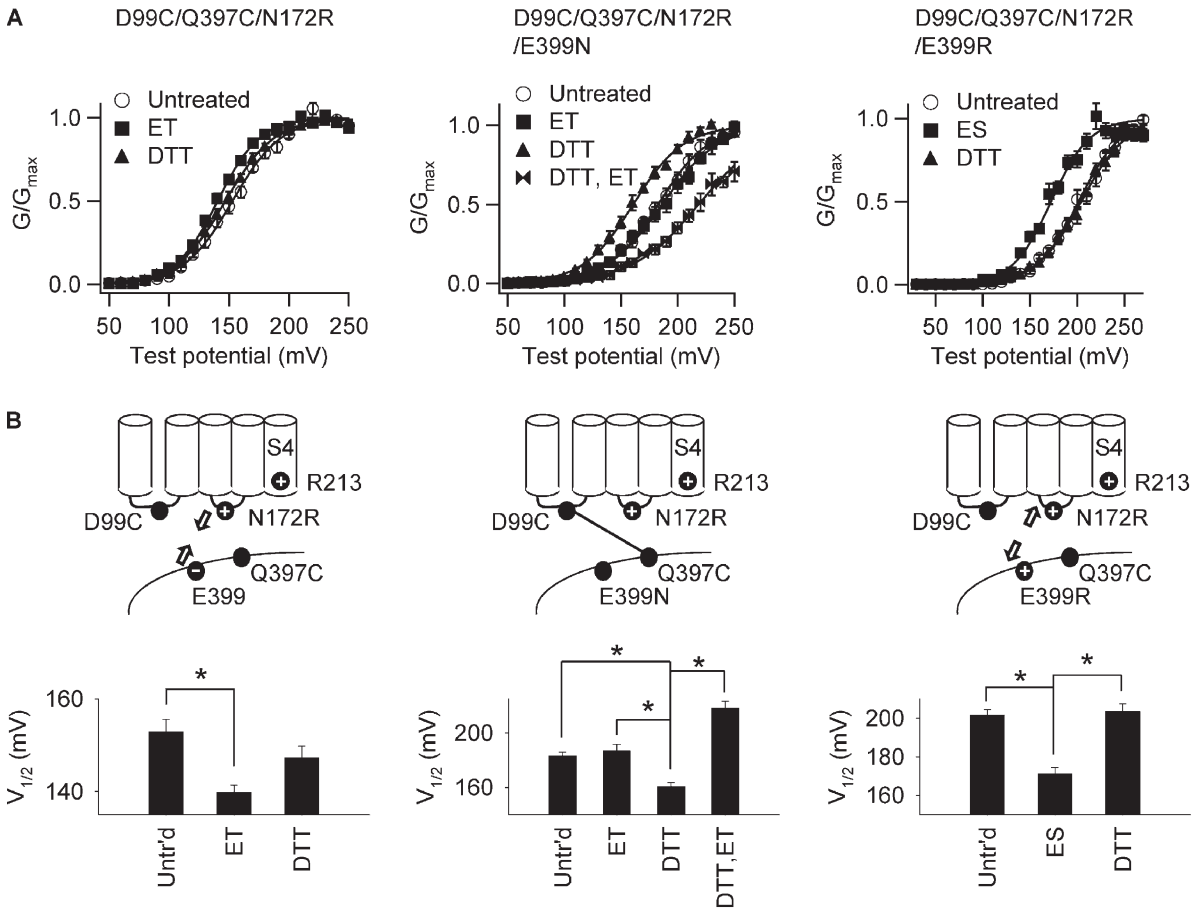

Figure 6. The 172–399 electrostatic interaction disrupts the formation of the interdomain disulfide bond. (A) G-V relations before (open circles) and after (closed symbols) treatment of MTSET (ET), MTSES (ES), or DTT when E399 is mutated to Asn (middle) or Arg (right) on the background of D99C/Q397C/N172R (left). "DTT, ET" in the middle panel represents the treatment of DTT followed by MTSET. $[Ca^{2+}]_i$: 0. Solid lines are fittings to the Boltzmann equation. The fitting parameters are: D99C/Q397C/N172R untreated ($n = 8$): $V_{1/2} = 153 \pm 3$ and $z = 1.3 \pm 0.02$; after ET ($n = 5$): $V_{1/2} = 140 \pm 2$ and $z = 1.37 \pm 0.04$; after DTT ($n = 6$): $V_{1/2} = 147 \pm 3$ and $z = 1.28 \pm 0.06$; D99C/Q397C/N172R/E399N untreated ($n = 6$): $V_{1/2} = 183 \pm 3$ and $z = 1.14 \pm 0.07$; after ET ($n = 8$): $V_{1/2} = 187 \pm 5$ and $z = 1.07 \pm 0.05$; after DTT ($n = 11$): $V_{1/2} = 161 \pm 3$ and $z = 1.26 \pm 0.04$; after DTT and ET ($n = 3$): $V_{1/2} = 218 \pm 5$ and $z = 0.88 \pm 0.06$; D99C/Q397C/N172R/E399R untreated ($n = 9$): $V_{1/2} = 202 \pm 3$ and $z = 1.20 \pm 0.03$; after ES ($n = 7$): $V_{1/2} = 171 \pm 3$ and $z = 1.33 \pm 0.07$; after DTT ($n = 8$): $V_{1/2} = 203 \pm 4$ and $z = 1.12 \pm 0.05$. (B) $V_{1/2}$ of the G-V relations shown in A for the corresponding mutations and chemical modifications. Cartoons on the top show the type of the 172–399 electrostatic interactions (arrows) as a result of residue 399 charges and its consequence on the formation of the disulfide bond between D99C and D397C (line) based on the results (see Results). Asterisks indicate significant difference between labeled pairs as identified in multiple comparisons ($P < 0.017$ for the left and right panels and $P < 0.0083$ for the middle panel as adjusted by the Bonferroni correction). All the mutations are on the background of C430A.

showed that the formation of the C99–C397 disulfide bond restricts channel activation; thus, breaking the disulfide bond by DTT treatment would facilitate channel activation (Yang et al., 2008). In addition, when C397 was modified by MTSET(+) or MTSES(−), the charge attached to C397 would interact with R213 in S4 to change channel activation (Yang et al., 2008), whereas the C99–C397 disulfide bond protects C397 from MTS modification so that MTSET(+) or MTSES(−) treatment should not alter channel activation. If no spontaneous disulfide bond is formed between C99 and C397, the thiol group on C397 will be available for MTSET(+) or MTSES(−) modification, resulting in a shift of G-V relation, whereas DTT treatment should no longer have any effect on G-V relation.

As shown in Fig. 6 (A and B, left), adding a positive charge to residue 172 (N172R) to the double cysteine mutation of D99C/Q397C made the resulting mutant channel no longer sensitive to DTT treatment but more activated after MTSET(+) treatment, suggesting that the electrostatic attraction between R172 and E399 prevented the spontaneous formation of the C99–C397 disulfide bond. Similar results were observed when converting the electrostatic interaction between residues 172 and 399 from attraction to repulsion by introducing two positively charged Arg residues to both sites (Fig. 6 A and B, right). In this experiment, we used MTSES(−) instead of MTSET(+) because a positive environment of N172R/E399R may potentially repulse the positively charged MTSET(+) to prevent it from modifying C397 (Elinder et al., 2001; D. Wu et al., 2010). These results indicate that both attractive and repulsive 172–399 interactions disrupt the spontaneous formation of the interdomain disulfide bond between C99 and C397. To further verify this, we abolished the 172–399 electrostatic interaction by removing the negative charge on residue 399 (E399N) of the D99C/Q397C/N172R triple mutant channel (Fig. 6, A and B, middle). The resulting D99C/Q397C/N172R/E399N channel can no longer be modified by MTSET(+), indicating the formation of the spontaneous disulfide bond between C99 and C397. Treating this mutant channel with DTT broke the disulfide bond and shifted the G-V relation to more negative voltages. The subsequent treatment with MTSET(+) shifted the G-V relation to even more positive voltages, further indicating the formation of the C99–C397 disulfide bond when the electrostatic interaction between residues 172 and 399 is absent. Collectively, the above chemical treatment experiments indicate that the electrostatic interaction between residues 172 and 399 can alter the distance or relative orientation between C99 and C397, thereby preventing the formation of the spontaneous disulfide bond. Therefore, the interaction between residues 172 and 399 induces conformational changes in the surrounding structures. It is worth noting that chemical modification resulted in a shallower slope of the G-V relation (Fig. 6). This is probably caused by incomplete modification such that the G-V relation is a mixture of the modified and intact channel species.

Electrostatic interaction between residues 172 and 399 alters intrinsic open probability of the pore

Besides its impact on channel activation by voltage and Ca^{2+}, the 172–399 interaction also alters intrinsic properties of the channel, such as the open probability of the activation gate in the absence of voltage-sensor activation and Ca^{2+} binding. Previous studies have shown that the BK channel conducts K^+ current with a small but finite P_o at 0 $[Ca^{2+}]_i$ and negative voltages (less than −80 mV) where the voltage sensors are at the resting state (Horrigan et al., 1999). Such an intrinsic P_o without activation of the sensors is determined by the properties of the pore-gate and its interaction with other structure domains and thus can be used to detect conformational changes in the pore-gate domain caused by the 172–399 interaction. The intrinsic P_o of BK channels is obtained by recording the unitary currents in a patch that contains hundreds of channels at negative voltages (less than −20 mV) (Horrigan et al., 1999; Cui and Aldrich, 2000) (Fig. 7 A). The P_o-V relation was then combined with the G-V relation at high voltages to generate the complete curve of P_o versus voltage (Fig. 7 B). Fig. 7 B (left) shows that on the WT background, where the native N172 is neutral, mutation E399R has no effects on BK channel P_o at any voltage range, indicating that P_o is not sensitive to the charge type at 399. However, on the N172D background, mutations E399N and E399R shift the voltage dependence of P_o toward more negative voltage ranges (Fig. 7 B, right), indicating that the electrostatic interaction between residues 172 and 399 alters voltage-dependent gating. Moreover, at extreme negative voltages (less than −80 mV), where P_o is independent of VSD activation, both repulsive (N172D) and attractive (N172D/E399R) 172–399 interactions lower P_o, whereas P_o is similar to that of the WT channel when there is no 172–399 electrostatic interaction (N172D/E399N) (Fig. 7, B, right, and C). By fitting the P_o-V relation to the HCA model (Eq. 2) (Horrigan et al., 1999), we obtained parameter L_0 (Fig. 7 D). L_0 is the open probability at 0 voltage without activation of the voltage sensor or Ca^{2+}-binding sites, which reflects the intrinsic property of the activation gate. We fitted the P_o-V relations to the HCA model with fixed parameters $z_L = 0.1$ and $z_J = 0.57$ to obtain L_0 (Fig. 7 D). The result shows that when there is no interaction between residues 172 and 399, L_0 is at the same level (WT, E399R, and N172D/E399N). However, both repulsive (N172D) and attractive (N172D/E399R) interactions lower L_0 (the difference is more than five times of the standard deviation of fitting), indicating that the intrinsic pore gate property is altered by the 172–399 electrostatic

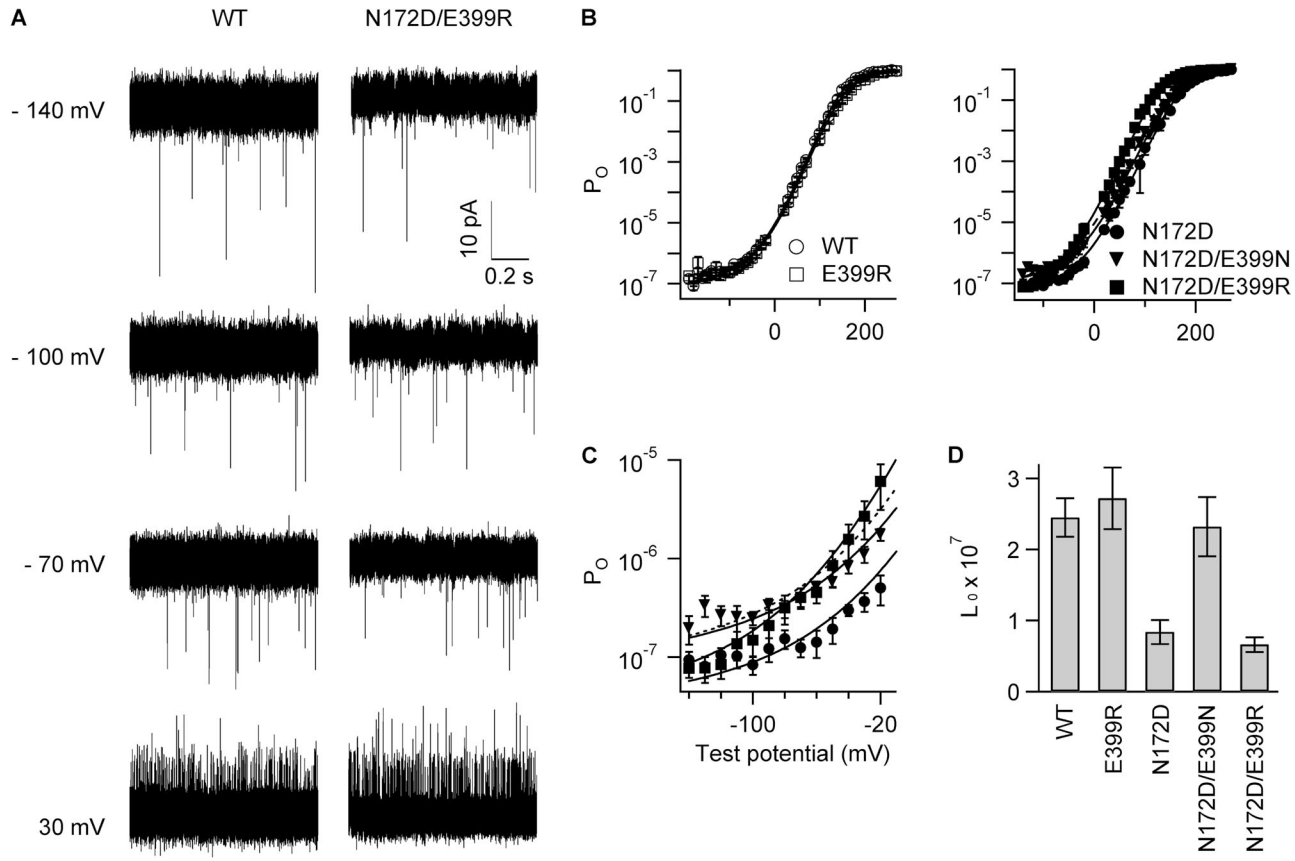

Figure 7. The 172–399 electrostatic interaction alters the intrinsic open probability of the activation gate. (A) Current traces of unitary openings (thin spikes) elicited by indicated voltages from inside-out patches expressing hundreds of channels. $[Ca^{2+}]_i = 0$. (B) P_O-V relation for WT and E399R (left), N172D, N172D/E399N, and N172D/E399R (right). $[Ca^{2+}]_i = 0$. Solid lines are fittings to the HCA model (Eq. 2) ($n \geq 5$). Dashed line in the right panel is the HCA fitting for WT. (C) Enlarged P_O-V relations in the right panel of B at the negative voltage range. (D) L_0 of the HCA model. Error bars represent 95% confidence intervals. The HCA model has fixed parameters ($z_L = 0.1$ and $z_J = 0.57$), whereas L_0, V_{hc}, and V_{ho} are optimized for the best fitting. V_{hc} and V_{ho} values (mV) are as follows (parameter ± 95% confidence interval): WT: $V_{hc} = 172 \pm 8$ and $V_{ho} = -18 \pm 3$; E399R: $V_{hc} = 164 \pm 9$ and $V_{ho} = -15 \pm 4$; N172D: $V_{hc} = 188 \pm 10$ and $V_{ho} = -11 \pm 4$; N172D/E399N: $V_{hc} = 173 \pm 9$ and $V_{ho} = -13 \pm 4$; N172D/E399R: $V_{hc} = 168 \pm 10$ and $V_{ho} = -54 \pm 3$.

interaction. Collectively, the 172–399 interaction not only alters the local conformation near the Mg^{2+}-binding site (Fig. 6) but also affects distant conformations including the pore-gate (Fig. 7). These conformational changes could interfere with the allosteric mechanisms of channel gating so that the voltage- and Ca^{2+}-dependent activation is altered as a result.

DISCUSSION

In this paper, a native interaction that participates in channel activation was identified between two of the Mg^{2+}-binding coordination residues, D99 and E374. To study the D99–E374 interaction while avoiding complications caused by interactions of these residues with those outside of the Mg^{2+}-binding site, we introduced artificial electrostatic interactions between the other two Mg^{2+}-binding coordination residues, N172 and E399, through mutagenesis and chemical modifications. The engineered 172–399 interactions mimic the native 99–374 interactions based on the following observations: (a) they are all part of the Mg^{2+}-binding site (Shi et al., 2002; Yang et al., 2008); (b) one partner of the interactions, D99 or N172, is located in the membrane-spanning domain, while the other, E374 or E399, is located in the cytosolic domain; and (c) electric charges on these residues are important for the interactions; opposite charges in either pair favor channel activation as compared with the like charges (Figs. 1 and 5). Our results show that the interactions between residues 172 and 399 affect both voltage- and Ca^{2+}-dependent activation through allosteric mechanisms. Such functional effects probably result from conformational changes that are proximal to the Mg^{2+}-binding site (Fig. 6) and distant from the pore-gate domain (Fig. 7).

Our current discovery of the noncovalent interactions between the interdomain Mg^{2+}-coordination residues may add new insights to the understanding of the allosteric mechanisms of BK channel gating. Our previous studies showed that Mg^{2+} bound to BK channels

interacts with R213 in the S4 segment to favor voltage-sensor activation, and this interaction is stronger when the channel is at the open state (Yang et al., 2007). Both of these properties contribute to Mg^{2+}-dependent activation of the channel. However, a recent study demonstrated that Mg^{2+} binding at the closed state also contributes to channel activation (Chen et al., 2011). Because the native interdomain interaction between D99 and E374 affects channel activation in the absence of Mg^{2+}, it is possible that Mg^{2+} binding can disturb such an interaction at either the closed or open state to facilitate channel activation.

These results may also help our current understanding of the allosteric Ca^{2+}-dependent activation of BK channels. Recent structural studies suggest that the cytosolic domain undergoes large conformational rearrangements upon Ca^{2+} binding (Yuan et al., 2012). Such a large conformational change in the cytosolic domain can open the gate in the membrane-spanning domain by pulling the C-linker that covalently connects these two domains (Niu et al., 2004; Yuan et al., 2012). Our current study illustrates that the noncovalent interactions between residues D99–E374 and charges at 172–399 in the Mg^{2+}-binding site can also affect Ca^{2+}-dependent activation (Fig. 5). Because the interacting partners, D99–E374 or charges at 172–399, are located on the membrane-spanning and cytosolic domains of the BK channel, respectively, the interactions are likely to change the interfacial conformations between the two domains. Such an interfacial conformational change is suggested by the results that the 172–399 interaction disrupts the spontaneously formed disulfide bond that cross-links the two structural domains between C99 and C397 (Fig. 6). Interfacial conformations between different structural domains have also been shown previously to be important for activation of various ion channels (Gordon et al., 1997; Jiang et al., 2002; Bouzat et al., 2004; Niu et al., 2004; Unwin, 2005; Long et al., 2007; Kawate et al., 2009; Taraska et al., 2009).

The noncovalent interactions at the interface between the membrane-spanning and cytosolic domains of BK channels might be much more complicated than the electrostatic interactions that we have shown in this work. For instance, charges at residue 172 still can affect channel activation when its cytosolic electrostatic partner E399 was neutralized (Fig. 4 B), suggesting that charges at residue 172 might be within an interaction network with other residues in vicinity. Considering the narrow distance between the membrane-spanning domain and the cytosolic domain, as well as the 71-residue-long S0–S1 linker that might squeeze into the interface, the interdomain noncovalent interactions, including electrostatic interactions, hydrophobic interactions, and hydrogen bonds, might tightly regulate the dynamic coupling of different structural domains to control BK channel gating. Our current study using electrostatic interaction as a tool to probe the interdomain interface will pave the way to further understand the domain–domain interactions and their effects on the allosteric gating mechanism of BK channels.

We thank Dr. Karl Magleby for helpful suggestions on the manuscript and Dr. Lawrence Salkoff for providing the mSlo1 clone.

This work was supported by National Institutes of Health (grants R01-HL70393 and R01-NS060706 to J. Cui). J. Cui is the Professor of Biomedical Engineering on the Spencer T. Olin Endowment.

Kenton J. Swartz served as editor.

Submitted: 21 February 2012
Accepted: 4 January 2013

REFERENCES

Adelman, J.P., K.-Z. Shen, M.P. Kavanaugh, R.A. Warren, Y.-N. Wu, A. Lagrutta, C.T. Bond, and R.A. North. 1992. Calcium-activated potassium channels expressed from cloned complementary DNAs. *Neuron.* 9:209–216. http://dx.doi.org/10.1016/0896-6273(92)90160-F

Bouzat, C., F. Gumilar, G. Spitzmaul, H.L. Wang, D. Rayes, S.B. Hansen, P. Taylor, and S.M. Sine. 2004. Coupling of agonist binding to channel gating in an ACh-binding protein linked to an ion channel. *Nature.* 430:896–900. http://dx.doi.org/10.1038/nature02753

Brayden, J.E., and M.T. Nelson. 1992. Regulation of arterial tone by activation of calcium-dependent potassium channels. *Science.* 256:532–535. http://dx.doi.org/10.1126/science.1373909

Butler, A., S. Tsunoda, D.P. McCobb, A. Wei, and L. Salkoff. 1993. mSlo, a complex mouse gene encoding "maxi" calcium-activated potassium channels. *Science.* 261:221–224. http://dx.doi.org/10.1126/science.7687074

Chen, R.-S., Y. Geng, and K.L. Magleby. 2011. Mg^{2+} binding to open and closed states can activate BK channels provided that the voltage sensors are elevated. *J. Gen. Physiol.* 138:593–607. http://dx.doi.org/10.1085/jgp.201110707

Cui, J., and R.W. Aldrich. 2000. Allosteric linkage between voltage and Ca^{2+}-dependent activation of BK-type mslo1 K^+ channels. *Biochemistry.* 39:15612–15619. http://dx.doi.org/10.1021/bi001509+

Cui, J., H. Yang, and U.S. Lee. 2009. Molecular mechanisms of BK channel activation. *Cell. Mol. Life Sci.* 66:852–875. http://dx.doi.org/10.1007/s00018-008-8609-x

Dudev, T., and C. Lim. 2003. Principles governing Mg, Ca, and Zn binding and selectivity in proteins. *Chem. Rev.* 103:773–788. http://dx.doi.org/10.1021/cr020467n

Elinder, F., R. Männikkö, and H.P. Larsson. 2001. S4 charges move close to residues in the pore domain during activation in a K channel. *J. Gen. Physiol.* 118:1–10. http://dx.doi.org/10.1085/jgp.118.1.1

Golowasch, J., A. Kirkwood, and C. Miller. 1986. Allosteric effects of Mg2+ on the gating of Ca2+-activated K+ channels from mammalian skeletal muscle. *J. Exp. Biol.* 124:5–13.

Gordon, S.E., M.D. Varnum, and W.N. Zagotta. 1997. Direct interaction between amino- and carboxyl-terminal domains of cyclic nucleotide-gated channels. *Neuron.* 19:431–441. http://dx.doi.org/10.1016/S0896-6273(00)80951-4

Hazes, B., and B.W. Dijkstra. 1988. Model building of disulfide bonds in proteins with known three-dimensional structure. *Protein Eng.* 2:119–125. http://dx.doi.org/10.1093/protein/2.2.119

Horrigan, F.T., and R.W. Aldrich. 2002. Coupling between voltage sensor activation, Ca^{2+} binding and channel opening in large conductance (BK) potassium channels. *J. Gen. Physiol.* 120:267–305. http://dx.doi.org/10.1085/jgp.20028605

Horrigan, F.T., J. Cui, and R.W. Aldrich. 1999. Allosteric voltage gating of potassium channels I. Mslo ionic currents in the absence of $Ca^{(2+)}$. *J. Gen. Physiol.* 114:277–304. http://dx.doi.org/10.1085/jgp.114.2.277

Hu, L., J. Shi, Z. Ma, G. Krishnamoorthy, F. Sieling, G. Zhang, F.T. Horrigan, and J. Cui. 2003. Participation of the S4 voltage sensor in the Mg^{2+}-dependent activation of large conductance (BK) K^+ channels. *Proc. Natl. Acad. Sci. USA.* 100:10488–10493. http://dx.doi.org/10.1073/pnas.1834300100

Jiang, Y., A. Lee, J. Chen, M. Cadene, B.T. Chait, and R. MacKinnon. 2002. Crystal structure and mechanism of a calcium-gated potassium channel. *Nature.* 417:515–522. http://dx.doi.org/10.1038/417515a

Kawate, T., J.C. Michel, W.T. Birdsong, and E. Gouaux. 2009. Crystal structure of the ATP-gated P2X(4) ion channel in the closed state. *Nature.* 460:592–598. http://dx.doi.org/10.1038/nature08198

Long, S.B., X. Tao, E.B. Campbell, and R. MacKinnon. 2007. Atomic structure of a voltage-dependent K+ channel in a lipid membrane-like environment. *Nature.* 450:376–382. http://dx.doi.org/10.1038/nature06265

Meredith, A.L., S.W. Wiler, B.H. Miller, J.S. Takahashi, A.A. Fodor, N.F. Ruby, and R.W. Aldrich. 2006. BK calcium-activated potassium channels regulate circadian behavioral rhythms and pacemaker output. *Nat. Neurosci.* 9:1041–1049. http://dx.doi.org/10.1038/nn1740

Niu, X., X. Qian, and K.L. Magleby. 2004. Linker-gating ring complex as passive spring and Ca^{2+}-dependent machine for a voltage- and Ca^{2+}-activated potassium channel. *Neuron.* 42:745–756. http://dx.doi.org/10.1016/j.neuron.2004.05.001

Oberhauser, A., O. Alvarez, and R. Latorre. 1988. Activation by divalent cations of a Ca^{2+}-activated K^+ channel from skeletal muscle membrane. *J. Gen. Physiol.* 92:67–86. http://dx.doi.org/10.1085/jgp.92.1.67

Robitaille, R., M.L. Garcia, G.J. Kaczorowski, and M.P. Charlton. 1993. Functional colocalization of calcium and calcium-gated potassium channels in control of transmitter release. *Neuron.* 11:645–655. http://dx.doi.org/10.1016/0896-6273(93)90076-4

Schreiber, M., and L. Salkoff. 1997. A novel calcium-sensing domain in the BK channel. *Biophys. J.* 73:1355–1363. http://dx.doi.org/10.1016/S0006-3495(97)78168-2

Shi, J., and J. Cui. 2001. Intracellular Mg^{2+} enhances the function of BK-type Ca^{2+}-activated K^+ channels. *J. Gen. Physiol.* 118:589–606. http://dx.doi.org/10.1085/jgp.118.5.589

Shi, J., G. Krishnamoorthy, Y. Yang, L. Hu, N. Chaturvedi, D. Harilal, J. Qin, and J. Cui. 2002. Mechanism of magnesium activation of calcium-activated potassium channels. *Nature.* 418:876–880. http://dx.doi.org/10.1038/nature00941

Taraska, J.W., M.C. Puljung, N.B. Olivier, G.E. Flynn, and W.N. Zagotta. 2009. Mapping the structure and conformational movements of proteins with transition metal ion FRET. *Nat. Methods.* 6:532–537. http://dx.doi.org/10.1038/nmeth.1341

Unwin, N. 2005. Refined structure of the nicotinic acetylcholine receptor at 4A resolution. *J. Mol. Biol.* 346:967–989. http://dx.doi.org/10.1016/j.jmb.2004.12.031

Wu, D., K. Delaloye, M.A. Zaydman, A. Nekouzadeh, Y. Rudy, and J. Cui. 2010. State-dependent electrostatic interactions of S4 arginines with E1 in S2 during Kv7.1 activation. *J. Gen. Physiol.* 135:595–606. http://dx.doi.org/10.1085/jgp.201010408

Wu, Y., Y. Yang, S. Ye, and Y. Jiang. 2010. Structure of the gating ring from the human large-conductance Ca^{2+}-gated K^+ channel. *Nature.* 466:393–397. http://dx.doi.org/10.1038/nature09252

Xia, X.-M., X. Zeng, and C.J. Lingle. 2002. Multiple regulatory sites in large-conductance calcium-activated potassium channels. *Nature.* 418:880–884. http://dx.doi.org/10.1038/nature00956

Yang, H., L. Hu, J. Shi, K. Delaloye, F.T. Horrigan, and J. Cui. 2007. Mg^{2+} mediates interaction between the voltage sensor and cytosolic domain to activate BK channels. *Proc. Natl. Acad. Sci. USA.* 104:18270–18275. http://dx.doi.org/10.1073/pnas.0705873104

Yang, H., J. Shi, G. Zhang, J. Yang, K. Delaloye, and J. Cui. 2008. Activation of Slo1 BK channels by Mg^{2+} coordinated between the voltage sensor and RCK1 domains. *Nat. Struct. Mol. Biol.* 15:1152–1159. http://dx.doi.org/10.1038/nsmb.1507

Yang, J., G. Krishnamoorthy, A. Saxena, G. Zhang, J. Shi, H. Yang, K. Delaloye, D. Sept, and J. Cui. 2010. An epilepsy/dyskinesia-associated mutation enhances BK channel activation by potentiating Ca2+ sensing. *Neuron.* 66:871–883. http://dx.doi.org/10.1016/j.neuron.2010.05.009

Yuan, P., M.D. Leonetti, A.R. Pico, Y. Hsiung, and R. MacKinnon. 2010. Structure of the human BK channel Ca^{2+}-activation apparatus at 3.0 Å resolution. *Science.* 329:182–186. http://dx.doi.org/10.1126/science.1190414

Yuan, P., M.D. Leonetti, Y. Hsiung, and R. MacKinnon. 2012. Open structure of the Ca^{2+} gating ring in the high-conductance Ca^{2+}-activated K^+ channel. *Nature.* 481:94–97. http://dx.doi.org/10.1038/nature10670

Zhang, G., and F.T. Horrigan. 2005. Cysteine modification alters voltage- and Ca^{2+}-dependent gating of large conductance (BK) potassium channels. *J. Gen. Physiol.* 125:213–236. http://dx.doi.org/10.1085/jgp.200409149

Zhang, G., S.Y. Huang, J. Yang, J. Shi, X. Yang, A. Moller, X. Zou, and J. Cui. 2010. Ion sensing in the RCK1 domain of BK channels. *Proc. Natl. Acad. Sci. USA.* 107:18700–18705. http://dx.doi.org/10.1073/pnas.1010124107

Zhang, X., C.R. Solaro, and C.J. Lingle. 2001. Allosteric regulation of BK channel gating by Ca^{2+} and Mg^{2+} through a nonselective, low affinity divalent cation site. *J. Gen. Physiol.* 118:607–636. http://dx.doi.org/10.1085/jgp.118.5.607